Analysis of the topology of Electromagnetic and Hadronic showers in the ECs and LACs of the CLAS

CLAS-NOTE 2004-032

Mark W.H. van Asseldonk, James W. Jury
Trent University, Peterborough, Ontario, Canada
The George Washington University, Washington, DC, USA

August 30, 2004

Abstract

Traditionally, γ and neutron initiated showers are distinguished in the electromagnetic and large-angle calorimeters of the CEBAF Large Acceptance Spectrometer (CLAS) by utilizing time-of-flight information to perform a β cut. It would be desirable to improve this method in order to create a more comprehensive technique for feasible particle identification. Therefore, the purpose of this study is to devise a complementary means to distinguish between electromagnetic showers and hadronic showers in the ECs and LACs. One possible technique involves utilizing shower topology characteristics such as shower widths and scattering angles to achieve this goal.

Contents

1 Introduction

Typically, γ and neutron initiated showers in the CEBAF Large Acceptance Spectrometer (CLAS) are discriminated using the time-of-flight (TOF) measurements that utilizes the β cut technique. The most basic difference between these showers is that the γ-ray and neutron initiated cascades are electromagnetic and hadronic respectively. One of the key features of the electromagnetic shower is its longitudinal and lateral size, which is dependent upon the characteristics of the composite material it cascades through [FABJ03]. It is also well known that hadronic showers typically have a larger lateral width than electromagnetic ones [ANZI93]. In the following study, GEANT simulated γ-ray and neutron showers events are analyzed in order to investigate an alternative or complementary method to the β cut procedure. This analysis focuses on using the topology of the shower as a comprehensive method for particle identification. The topology characteristics include the widths of the particle showers and scattering angles in the electromagnetic calorimeters and large angle calorimeters. This report is a summary of Mark W.H. van Asseldonk's summer undergraduate study which took place between July/Aug. 2003 at the Thomas Jefferson Laboratory Nuclear Accelerator Facility in Hall B of CLAS.

2 A shower-finding algorithm incorporating GEANT3 for analysis

For the following study a nuclear physics analysis program was written that utilized the GEANT3 library. The main component of the program is a shower-finding algorithm [JUEN03], which maps out the entire reaction history by analyzing all tracks that produce further reaction vertices. This algorithm seen schematically in Fig. 1 is the central component of the program. It is used to develop further the three major functionalities of the program, which include the analysis of the interaction vertices, the detector hits, and the shower identification. A hit is referred to as the information recorded at the tracking time when an interaction occurs between a particle and a particular detector. A hit is necessary to compute a digitization which is the detector response after tracking a complete event [BRUY86]. The simulation software package, GEANT3, greatly assisted the development of the program by providing prewritten and tested routines. The GEANT3 routines make accessing data simple and user friendly thus allowing the pro-

grammer to create an effective analysis program without having extensive prior knowledge of the software. For instance, a simple call of a routine such as GFKINE needs only a specific track number in order to produce a vast amount of kinematic data. Typically, these include the following: the 4-momentum, the particle track information, the vertex origin of the track, and the particle identification.

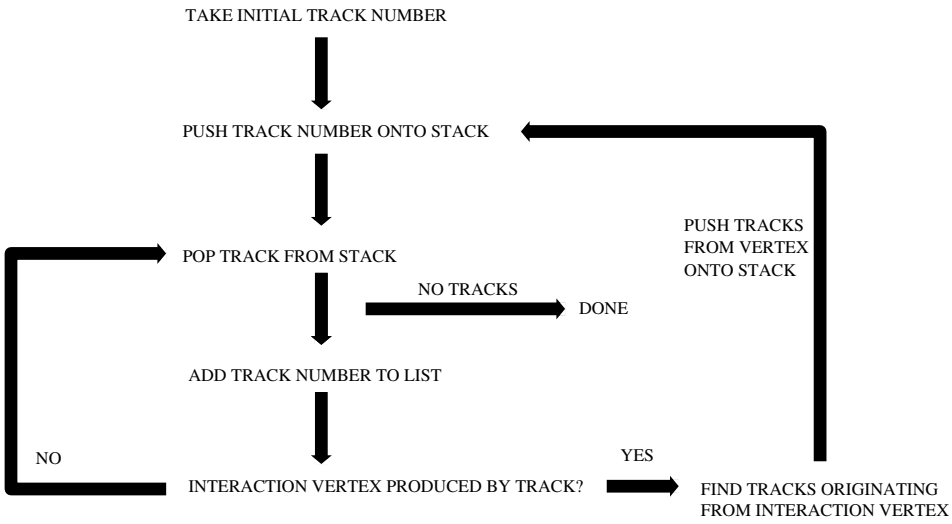

Figure 1: For each shower the analysis program conducts an essential algorithm which defines all the tracks and interaction vertices. Shown graphically is the algorithm's step by step process for mapping out an entire shower.

The shower-finding algorithm is initialized by taking the first track number and pushing it onto a stack. Then using a loop, the top track number is taken off of the stack. First, the track number is recorded in a track list. Second, it is analyzed in order to check whether at the end of the track an interaction vertex is produced. If no vertex is created the program loops back and prepares to pop the next track number from the top of the stack. However, if an interaction vertex is produced, the algorithm finds the new tracks originating from the point. All the newly found tracks are pushed one by one onto the top of the stack. Third, the program proceeds to the beginning of the loop. The algorithm continues to loop in this fashion, pushing and popping until there are no more tracks on the stack. Thus, a

complete track list is constructed.

3 Simulation and analysis of reactions

The analysis is based on the following reactions:

$$\gamma p \rightarrow p\pi^+\pi^-\pi^0 \quad (1)$$

$$\gamma p \rightarrow p\pi^0 \quad (2)$$

$$\gamma p \rightarrow n\pi^+ \quad (3)$$

$$\gamma p \rightarrow p\pi^+\pi^- \quad (4)$$

These reactions are of particular usefulness for an analysis program, because final state products such as pions, protons, and neutrons are included. Reactions (1) and (2) contain a π^0 which decays immediately via the $\pi^0 \rightarrow \gamma\gamma$ or $\pi^0 \rightarrow \gamma e^+e^-$ mechanisms. The branching ratios for these two channels from the Particle Data Group (PDG) are experimental values of (98.798 +/- 0.032)% and (1.198 +/- 0.032)% respectively [GROO00]. Since the simulations are carried out using the GEANT3-based event simulator the program could be easily readjusted for other various targets, such as deuterium or helium isotopes. The showers caused by the reaction products are ordered and interpreted by the analysis program developed for this study. The possible reaction products incorporated in the analysis program include the p, π^0, π^+, π^-, and n particles. Other desired reaction products could also be analyzed by adding the appropriate GEANT particle-bank information to the program, assuming the accompaniment of an appropriate event generated data set. The analysis program includes a specialized procedure to allow the user to study characteristics of both electromagnetic and hadronic showers.

4 Pertinent detector descriptions

The CLAS detector sets included in the analysis are: the drift chambers (DC), the forward electromagnetic calorimeter (EC), the large-angle electromagnetic calorimeter (LAC), the TOF scintillators (SC), the start counters (ST), and the Čerenkov Counters (CC). The two detectors of particular focus in the following study are the ECs and LACs. Both of these detectors are effective in tracking radiative decays, from particles such as π^0 and η [AMAR01]. The ECs reside in all six sectors of CLAS, while the LACs are

present in only two sectors. The EC detectors are used to detect electrons, gamma rays above 0.2 GeV and neutrons [AMAR01]. Note that the actual lower photon energy limit of the ECs is much less, but the efficiency drops dramatically for photon energies below 0.1 GeV. Photon angular acceptance within the CLAS environment is up to 45°. These ECs can be broken down in six calorimeter detector modules that include U-In, U-out, V-In, V-Out, W-In, W-Out. Each module contains 216 photomultiplier tubes (PMT) and thus CLAS has a total of 1296 PMTs in the ECs [AMAR01]. The EC modules are layers of lead and plastic scintillators stacked in sets of two, (eg. U-In, U-Out); thereby, these detectors form three parallel running planes through which showers can be tracked. Although the planes are parallel, the strips contained in the modules are not, otherwise no detection would occur. In fact, the strips are rotated by 120° for each successive layer [MECK03]. The LACs detect the same particles as the ECs but cover an azimuthal range of 120° and an angular scattering range of 45° to 75°. The two LACs are composed of two modules which contain 33 layers, each composed of a lead foil and a NE110A plastic scintillator bar. Within the scintillator the bars are placed such that each consecutive layer is rotated by 90°; thus, a 40 x 20 matrix of cells are formed [MECK03]. Both the EC and LAC detectors are read out by photomultiplier tubes (PMTs). The signal times of the PMTs are determined by FASTBUS time-to digital converters (TDCs) and the pulse heights are converted utilizing analog-to digital converters (ADCs). High resolution TDCs are required in order to have accurate time of flight measurements (TOF), while the ADCs are used to determine the energy deposited in the various detectors and to correct the TDCs for time walk [MECK03].

An example of a reaction and a complete shower going through a cross section of sectors 1 and 4 of CLAS is shown in Fig. 2. The shower events produced in this figure are the result of reaction (1). Two ECs and an LAC can be seen in this cross section of CLAS. This particular event illustrates a hadronic shower occurring in the upper right EC and two electromagnetic showers in the lower right EC.

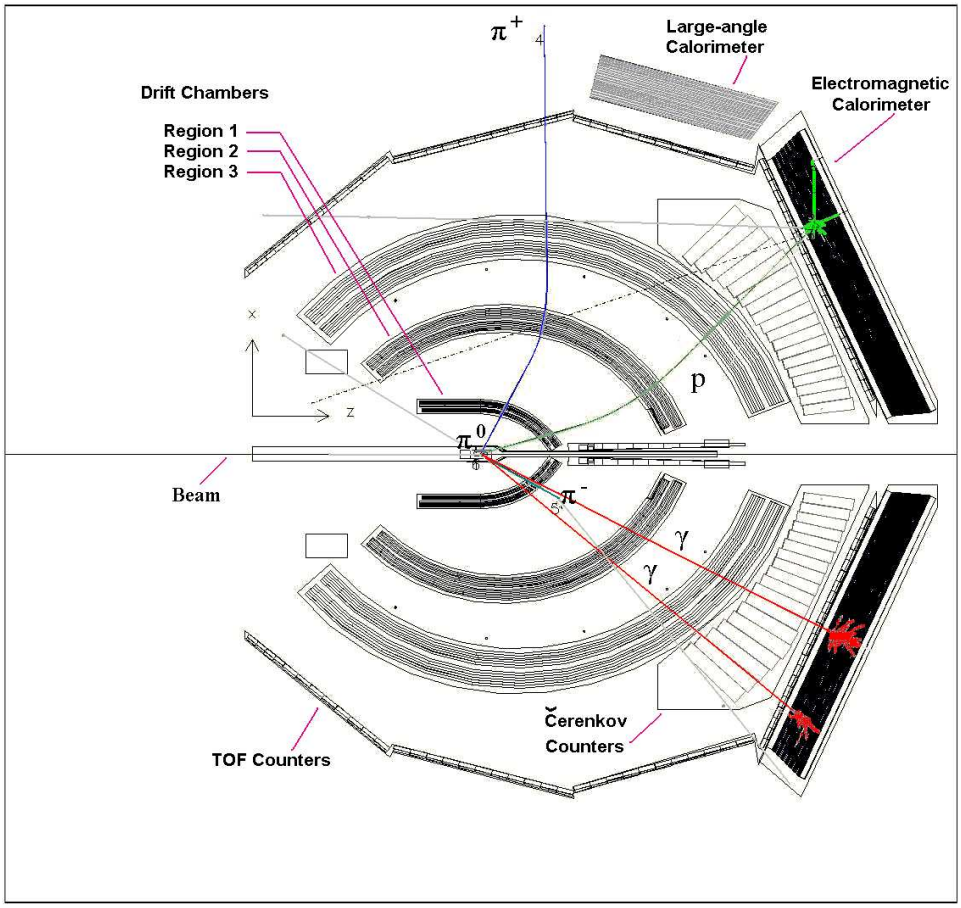

Figure 2: An example of reaction (1) in sectors 1 and 4 of CLAS [JUEN03]. For this particular event both an electromagnetic and a hadronic shower are shown hitting the electromagnetic calorimeters. The π^0 decay causes a γ-pair to be produced that creates two EM showers in the bottom right EC. The shower in the top right EC is a hadronic shower initiated by the outgoing proton.

5 Interaction of gammas with CLAS detector material

Interaction vertices were produced by particles that interacted with material contained in the CLAS detector. These interactions are not solely composed of the actual detector components such as the EC, DC, LAC, SC, and ST. As well, they include the interactions with the magnets, the gaseous particles inside the DC or between the detectors, or DC material such as the wires and walls. Such hits typically result in a single DC hit or a small cluster of DC hits. More important are the showers caused by direct hits of reaction products with the ECs and LACs. It will be the statistics of these hits that will be used to the differentiate between showers initiated by γ-rays and neutrons.

In Fig. 3 the CLAS detector is depicted through interaction vertices simulated by γ, π^-, π^+, and p particles from reaction (1). The space shown in the plots are defined by the Z axis (beam line going downstream), Y axis (vertical), and X axis (horizontal). The CLAS environment is outlined by the interactions to give a 3D view of the entire detector. Notice the six distinct main torus coils which can be seen surrounding the beam target at the origin of the plot. As well, a ring-like structure is evident upstream of the coils. This represents the metal support structures that exist in CLAS. In the top left of Fig. 3, the intense regions above or left of the magnets represent areas where the photons are interacting with the EC, LAC and CC. The white lines which cut through these intense areas are gaps where no detector exists and which are masked by the magnet coils.

Another informative view of the CLAS geometry is a projection in the X-Y plane. This view portrays a downstream depiction of the beamline seen in the top left of Fig. 4. Blind areas of the CLAS are illustrated by the six line white star region produced where the magnets are present. The intensely dark triangular regions are mainly due to the interaction vertices with the shower detectors. An alternative view is shown in the top right Fig. 4 which depicts the relative frequency of interactions.

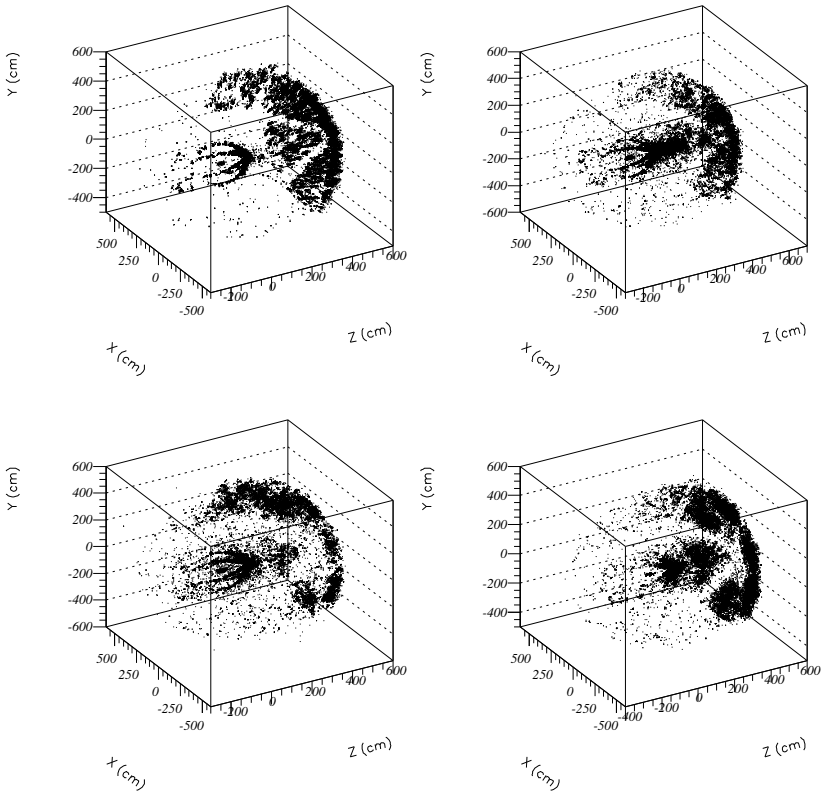

Figure 3: This plot shows the interactions of γ (top left), π^- (top right), π^+ (bottom left), and p (bottom right) from reaction (1) with the material present in CLAS.

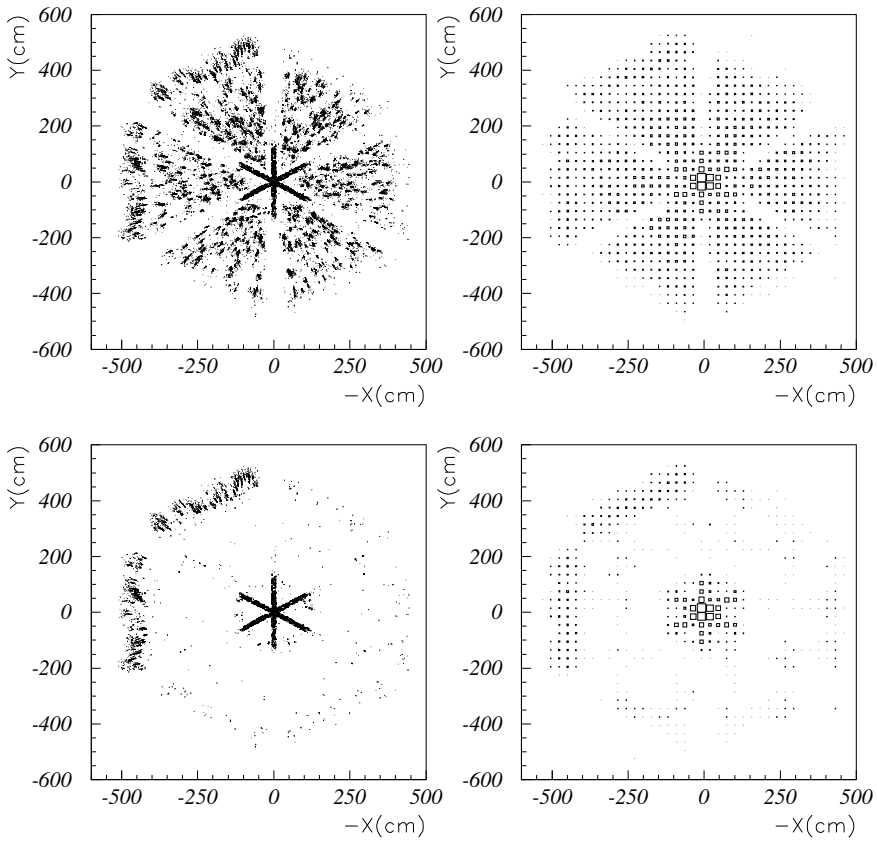

Figure 4: A downstream view of the CLAS beamline is created by the interactions of γ-rays. The top left diagram is useful for showing the configuration of the ECs, LACs, and mini-magnet torus. The figure to the top right is similar except it displays the relative frequency of interactions. In the bottom figures a cut is applied at 350 cm along the beamline so that the interactions with the EC would not be present. Notice how few γ interaction vertices remain after this cut.

A graphical plot of the beamline indicates with which detectors and CLAS components the γ-rays are mainly interacting. This view of CLAS is shown in Fig. 5; notice that three major peaks of interaction exist. The first peak around 0 cm represents the beam target and its encasing. The second major peak between 50-150cm represents the interactions of γ-rays with the magnetic torus coils. These coils are kidney-shaped and have a diameter of 5m and a length of 5m [MECK03]. For the third peak, consider again the downstream views of the detector in the top left and right of Fig. 5. If a graphical cut is applied to Fig. 5 at 350cm along the beam line, one can see the resulting less intense downstream view of the detector in the bottom of Fig. 4. The resulting plots do not display the major interactions with the ECs in the old downstream plots.

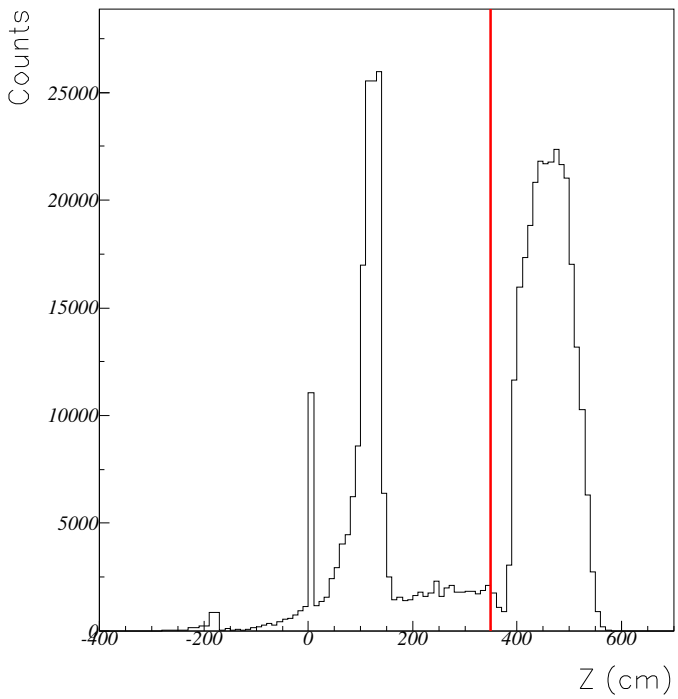

Figure 5: The γ interactions with material along the Z beamline of CLAS are displayed above. Notice if a cut is applied at 350 cm in this plot (indicated by the vertical line) then the interactions with the EC would not be present.

6 Interaction of charged particles with CLAS material

Particle characteristics such as charge, mass, and collision cross section cause distinct interaction patterns within CLAS. The top right of Fig. 3 illustrates the interactions caused by the π^- particles from reaction (1). Due to the polarity of the magnets in the CLAS detector it is evident that the negatively charged pions have a tendency to converge towards the direction of the Z-axis. As a result, the CLAS detector loses more π^- particles due to increased convergence at the blind spot downstream of the beam line. If the magnetic polarity were reversed, then more of the products of reaction (1) would be lost since the entire reaction has an overall charge of $+1$. The oppositely charged π^+ and p particles seen respectively in the bottom left and bottom right of Fig. 3, diverge more from the Z-axis. However, protons cause significantly more interaction vertices in the forward direction compared to the π^+ particles because of its larger collision cross section at higher momenta.

Charged particles are typically detected using the drift chambers. However, another interesting area of investigation is the effect of charged particles interacting with the ECs and LACs. Figure 6 shows the interactions of protons, π^+, and π^- particles down the beamline of CLAS. From the products of reaction (1), protons would create the largest hadronic showers in the ECs and LACs due to their high forward momentum dependence. Although charged particles are effectively detected by the drift chambers, hadronic showers initiated by charged particles in the ECs and LACs could be utilized to provide checks with the DCs or look for missing tracks.

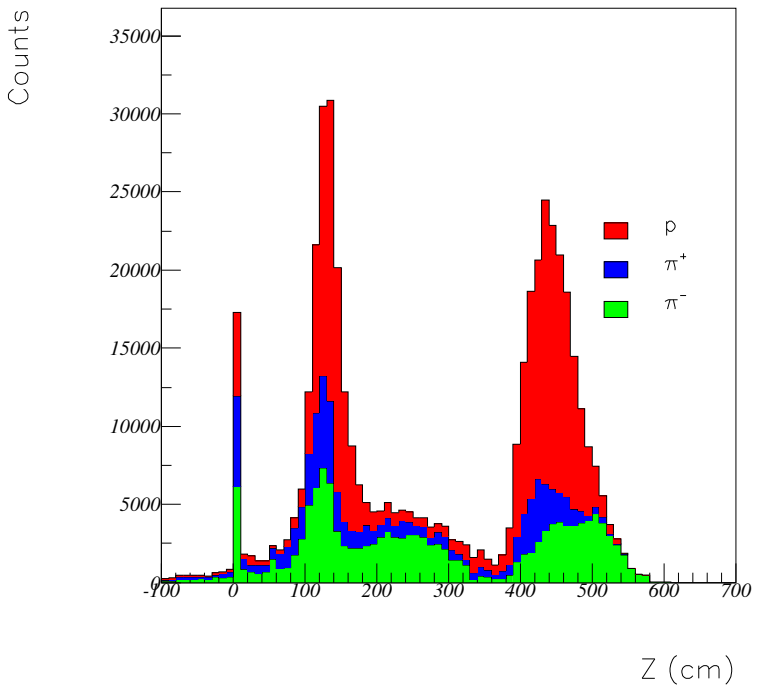

Figure 6: The charged particle interactions with material along the Z beamline of CLAS are displayed above for p, π^+, and π^- from reaction (1).

7 Selective analysis of CLAS shower content

Reaction products are created when a target is continuously bombarded by a high energy photon source. The particles produced by this initial collision can then interact with subsequent CLAS material to produce hadronic and EM showers. Photons interact to produce secondary gammas by bremsstrahlung, or secondary positrons and electrons via pair production [FABJ03]. The secondary particles in EM showers produce more particles by the same mechanism, which in turn creates more particles. This process continues creating a large cascade of increasing EM particles until the energy of the electrons within the shower degrade below a critical energy. Hadron showers proceed in a similar fashion, except for the fact that the cascades are produced by mostly strong interactions until there is insufficient energy to produce any further interaction products. One functionality of the analysis program developed in this study is to allow the user to select a reaction product and view the shower particles it produces in CLAS. For instance, in reaction (3) one can look at neutrons, and π^+, particles that interact with the ECs like in the top right of Fig. 7 or the LACs in the top left of Fig. 7 to cause showers. Similar can be shown in the bottom of Fig. 7 for γ-rays and protons from reaction (3). The arrangement of the particles on the horizontal axis is based on the numbering system of the GEANT particle banks. Not displayed but also available are the smaller quantities of products such as deuterons, tritons, and alpha particles. The selective nature of the analysis program allows the user to specify any area of initial detector interaction in CLAS caused by reaction products and any area of shower detection for subsequent cascades produced by these particles. The selectivity of the analysis program is especially helpful when examining the contents and topology of the showers. For instance, it is confirmed from the bottom of Fig. 7 that EM showers in the ECs and LACs initiated by γ-rays contain e^+, e^-, γ shower particles as should be expected. While hadronic showers initiated by neutrons, contain significant numbers of e^+, e^-, γ, p, and n shower particles as seen in the top of Fig. 7. But this same hadronic shower also contain trace amounts of pions and positively charged muons. These same specifications can be made when investigating the characteristics such as the shower widths and scattering angles.

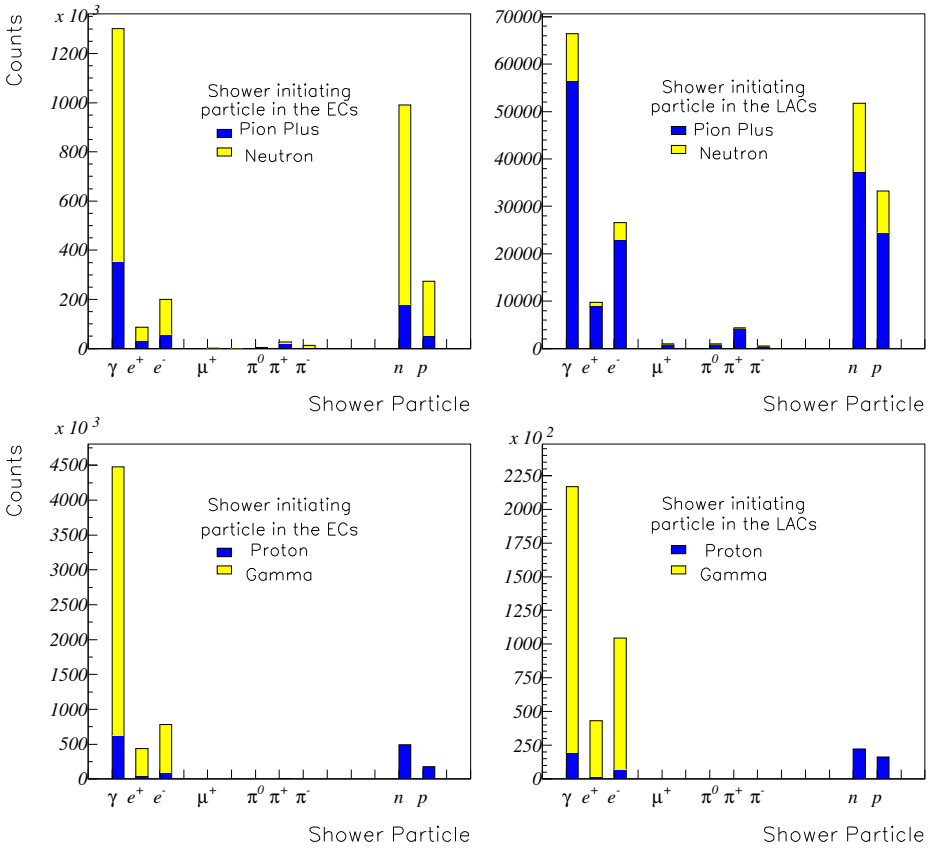

Figure 7: The contents of showers initiated by n and π^+ particles from reaction (3) are shown for the ECs and LACs in the top right and left figures respectively. While the contents of shower caused by γ-rays and protons from reaction (2) are shown for the ECs and LACs in the bottom right and left respectively.

8 Analysis of shower particle widths

The broadness and frequency of showers initiated in the ECs and LACs by hadrons, mesons, and photons and their corresponding shower particles is an area of interest. The major goal of this study was to distinguish between showers caused by neutrally charged gammas and neutrons. Traditionally, γ-n discrimination is achieved through time-of-flight measurements. However neutron detection efficiency, is zero at 0.4 GeV/c and rises to a plateau of 60% above 1.6 GeV/c in the ECs. Neutrons are separated from photons under 1.5 GeV/c by requiring a β cut of 0.9 is used [AMAR01]. The other detector system of interest is the LACs, which have an efficiency of 30% for momenta greater than 0.5 GeV/c. To distinguish gammas and neutrons under this energy a β cut of 0.95 is applied [MECK03]. Thus, an effective complementary means of discriminating between n and γ initiated showers in the ECs and LACs could involve utilizing shower-width statistics. The lateral dimension of hadronic and electromagnetic showers have been previously used to successfully discriminate between electrons and pions in different prototypes of a lead/scillating fibers calorimeter, at approximately 50 GeV [ANZI93].

To study showers in the ECs and LACs the analysis program was designed to focus specifically on the first interaction vertex that would lead to a shower in CLAS. An algorithm similar to the shower-finding algorithm mapped out the location of the hits caused by the shower starting from the shower origin. A basic diagram illustrating an interaction with material causing a shower is depicted in Fig. 8. If the particles traveling along the branches are detected then hits are registered on the tracks. Next a hypotenuse is defined from the shower initiating particle to each individual hit track point. A virtual line is defined in the direction of the momentum of the shower initiating particle. The depth of the shower is the length that lies along the direction of the momentum of the initial shower producing particle. It is a component of the projecting hypotenuse which connects the primary interaction vertex and a hit location. The width is defined as the component of the hypotenuse that connects at a right angle to the depth of the shower. Note that shower widths quoted in this study are the average of all the widths at full width half maximum.

From Fig. 9 and Fig. 10 it is evident that γ-ray initiated shower particles occur substantially in regions under 5 cm for both the ECs and LACs,

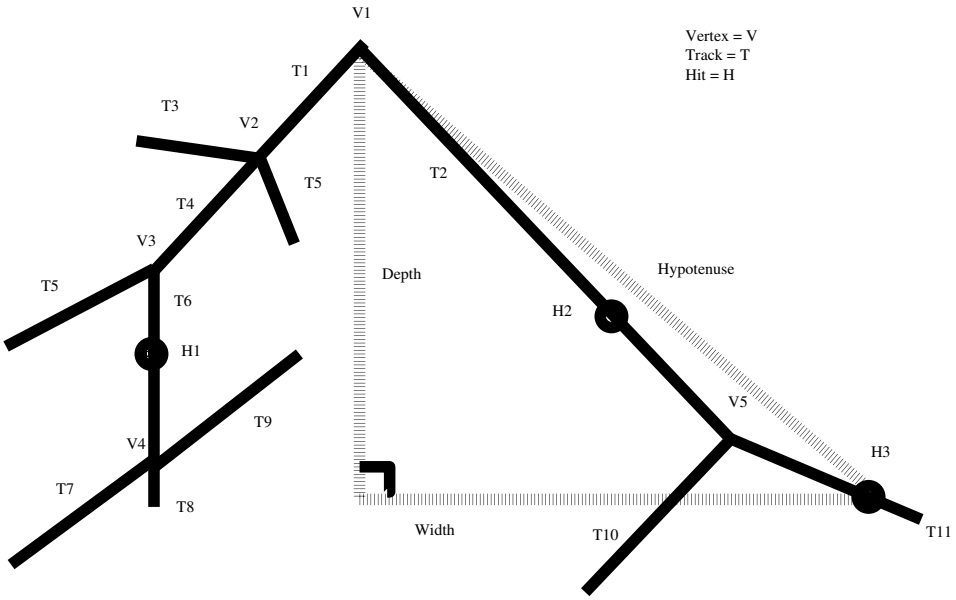

Figure 8: The following is a diagram which depicts and interaction vertex V_1 and the shower which emerges from this point. This diagram explains the analysis terminology used to describe the topology of showers. A hypotenuse could be pictured from V_1 to a hit in a detector such as H_3. The depth and width of the shower are defined as the horizontal and vertical component of the hypotenuse.

while hadrons and mesons produced shower widths exist in substantially frequencies over a much larger range. A close-up of this width range is seen in Fig. 11 and 12 for the ECs and LACs respectively. The symmetric nature of the γ distribution is an artifact due to the momentum distribution of the original simulated data. However, if one analyzes projections of the shower widths this artifact rapidly disappears and is of little influence to the shower data. In Fig. 9 - 12, a cut of widths less than 0.01 cm and 0.001 cm were applied to the ECs and LACs respectively to eliminate low energy shower particles. This cut was applied simply to illustrate the frequency of shower widths over a broader range.

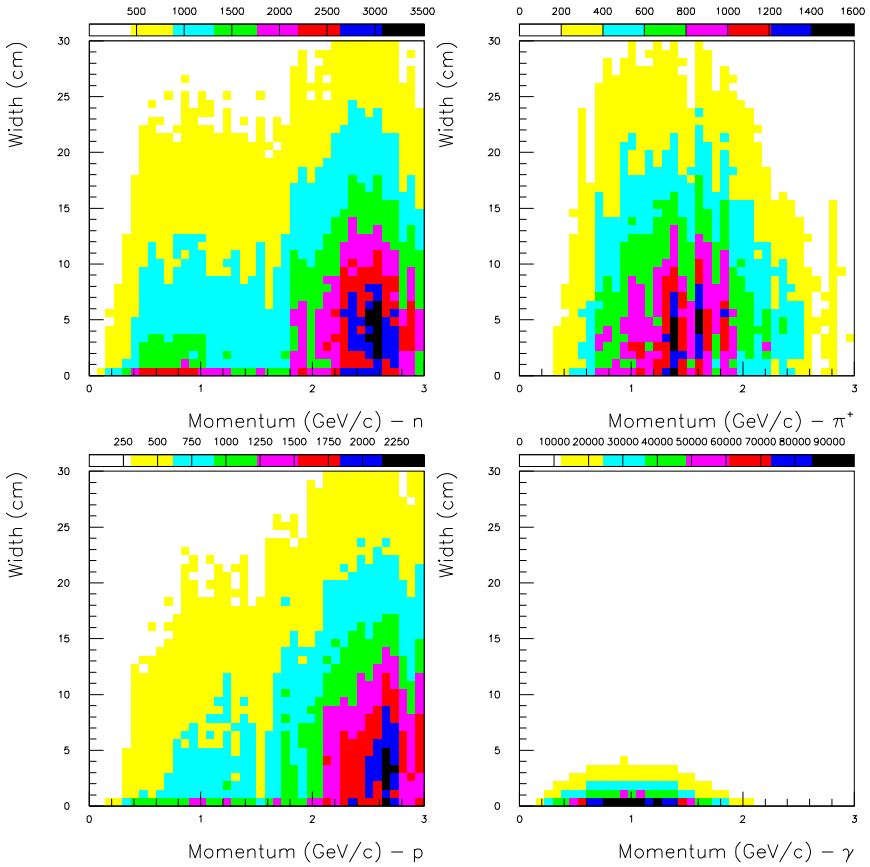

Figure 9: In the following plot showers are initiated by the products of reaction (2) and (3) in the EC. A range of showers of widths between (0-30)cm are plotted against a reaction product particle momentum range of (0-3) GeV/c. The reaction product particles causing the showers are n, π^+, p, and γ particles in the top left, top right, bottom left, and bottom right respectively.

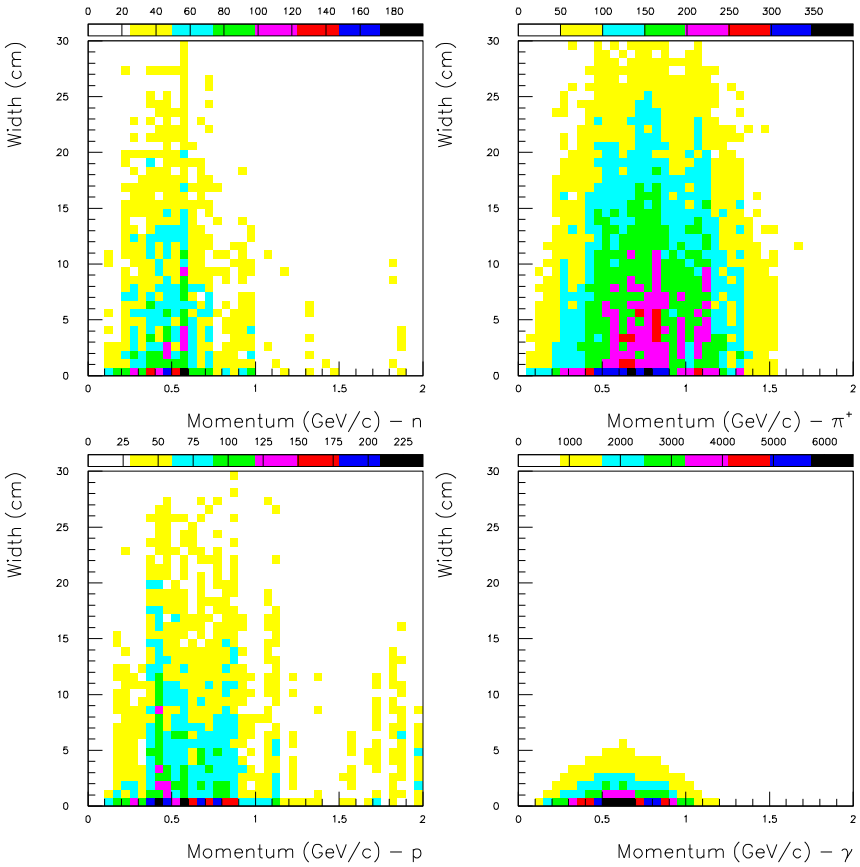

Figure 10: In the following plot showers are initiated by the products of reaction (2) and (3) in the LAC. A range of showers of widths between (0-30)cm are plotted against a reaction product particle momentum range of (0-2) GeV/c. The reaction product particles causing the showers are n, π^+, p, and γ particles in the top left, top right, bottom left, and bottom right respectively.

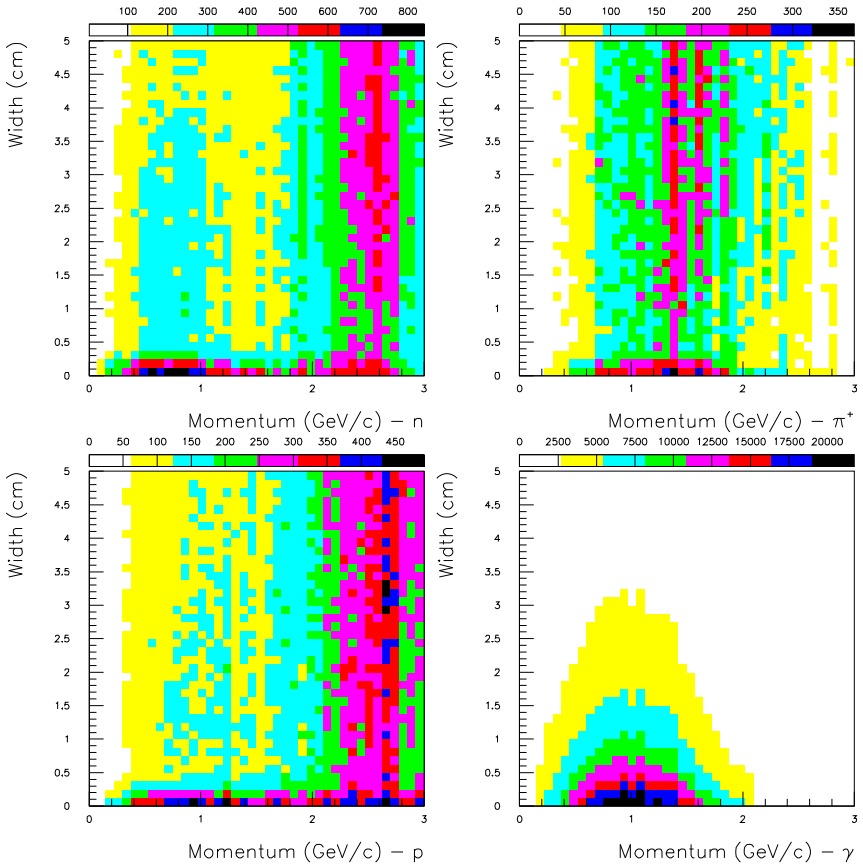

Figure 11: In the following plot showers are initiated by the products of reaction (2) and (3) in the EC. A range of showers of widths between (0-5)cm are plotted against a reaction product particle momentum range of (0-3) GeV/c. The reaction product particles causing the showers are n, π^+, p, and γ particles in the top left, top right, bottom left, and bottom right respectively.

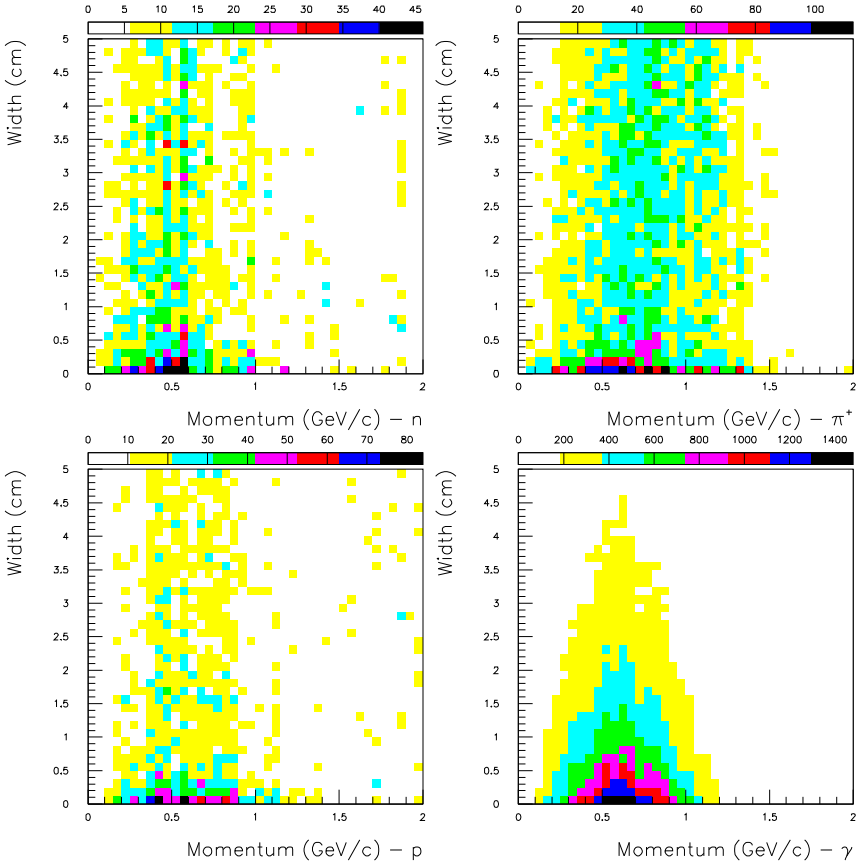

Figure 12: In the following plot showers are initiated by the products of reaction (2) and (3) in the LAC. A range of showers of widths between (0-5)cm are plotted against a reaction product particle momentum range of (0-2) GeV/c. The reaction product particles causing the showers are n, π^+, p, and γ particles in the top left, top right, bottom left, and bottom right respectively.

In order to analyze the showers in an accurate manner, it is necessary to examine the various momentum ranges of the shower initiating particle. Therefore, shower properties were investigated over low, medium, and high momenta ranges. These arbitrary momentum classifications were defined in 1.0 GeV/c increments. The momenta bands of each of these shower initiating particles are seen in Fig. 13. One major goal of this study was to detail the topology of showers initiated by neutral γ-rays and neutrons. Therefore, to contrast the topology of these particles, overlapping momentum ranges described as "low"(0-1 GeV/c), "medium" (1-2 GeV/c), and "high" (2-3 GeV/c) ranges were defined. It should be noted that gammas from the simulated data set have negligible frequency for momenta over 3 GeV/c. However, the dependence of shower topology on the shower initiating particle absolute momenta makes this classification necessary.

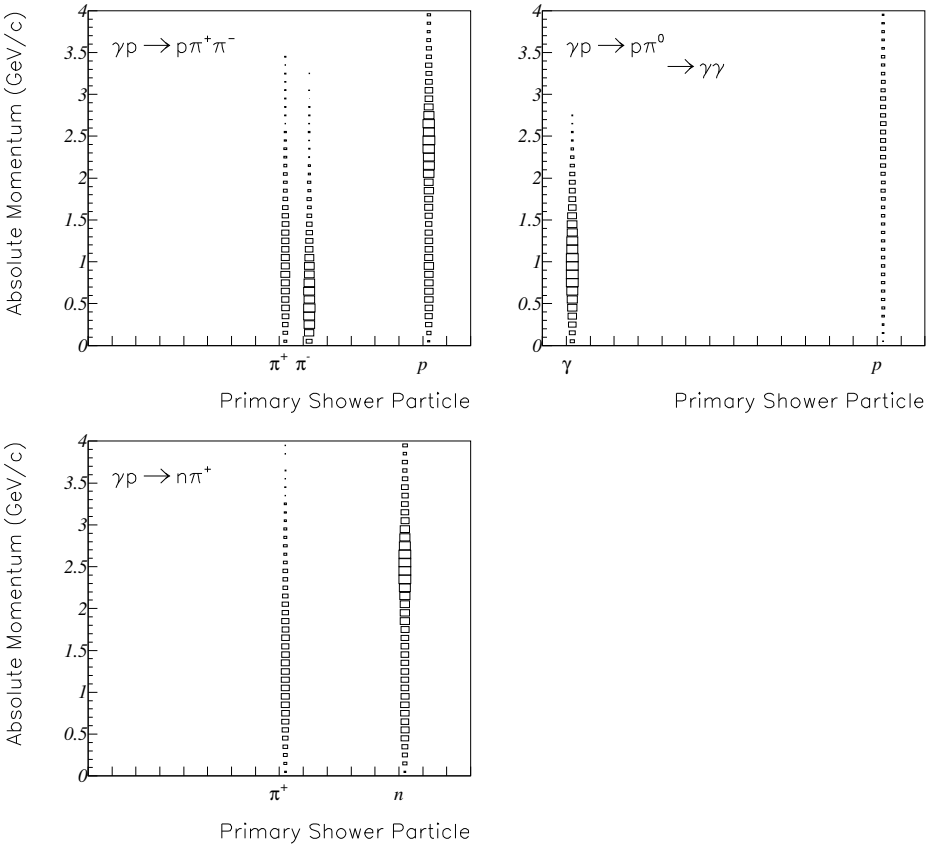

Figure 13: The following is a diagram which depicts the momentum bands of the products from three reaction (2), (3), and (4). These reaction products in turn could be shower initiating particles depending on how and where they interact in CLAS.

The following tables detail the average (AVG) and the root mean square (RMS) particle shower widths. Since γ showers are mainly composed of e^+, e^-, and γ components, no other individual shower particles were included. The average particle shower width in the ECs and LACs caused by gammas and neutrons are given in Tables (1) and (2). Note that primary shower-initiating particles in the LACs do not exist in sufficient numbers to quote meaningful statistics in the high momenta ranges. The statistics in Table (1) for the ECs and LACs were derived from the width projections seen in Fig. 14 and Fig. 15 respectively. Similarly, the statistics in Table (2) for the ECs and LACs are obtained from the width projections in Fig. 16 and Fig. 17 respectively.

		Width (cm)				
		ECs			**LACs**	
Particles	Statistic	**Low**	**Med**	**High**	**Low**	**Med**
γ	AVG	6.2	6.2	4.5	5.9	5.6
	RMS	5.4	5.1	6.8	7.5	7.5
e^+	AVG	3.0	1.7	1.5	2.6	2.2
	RMS	2.6	2.4	2.5	3.9	3.4
e^-	AVG	3.9	3.8	2.8	5.0	4.8
	RMS	4.8	4.8	5.2	6.5	6.6
All	AVG	6.1	6.0	4.3	5.3	5.1
	RMS	5.1	4.8	6.3	3.9	6.9

Table 1: The average width of showers (cm) in the ECs and LACs caused by gammas from the decay of the π^0 in reaction (2).

		Width (cm)				
		ECs			**LACs**	
Particles	Statistic	**Low**	**Med**	**High**	**Low**	**Med**
γ	AVG	21.5	22.5	19.5	20.1	22.2
	RMS	39.0	35.9	32.8	27.5	34.5
e^+	AVG	21.8	18.5	13.9	18.9	25.0
	RMS	40.4	30.5	20.4	22.8	47.2
e^-	AVG	21.8	22.4	18.1	20.7	23.4
	RMS	38.8	36.0	30.7	25.8	31.6
All	AVG	21.4	22.6	20.1	17.7	20.0
	RMS	37.8	35.0	33.0	24.1	29.1

Table 2: The average width of showers (cm) in the ECs and LACs caused by neutrons from reaction (3).

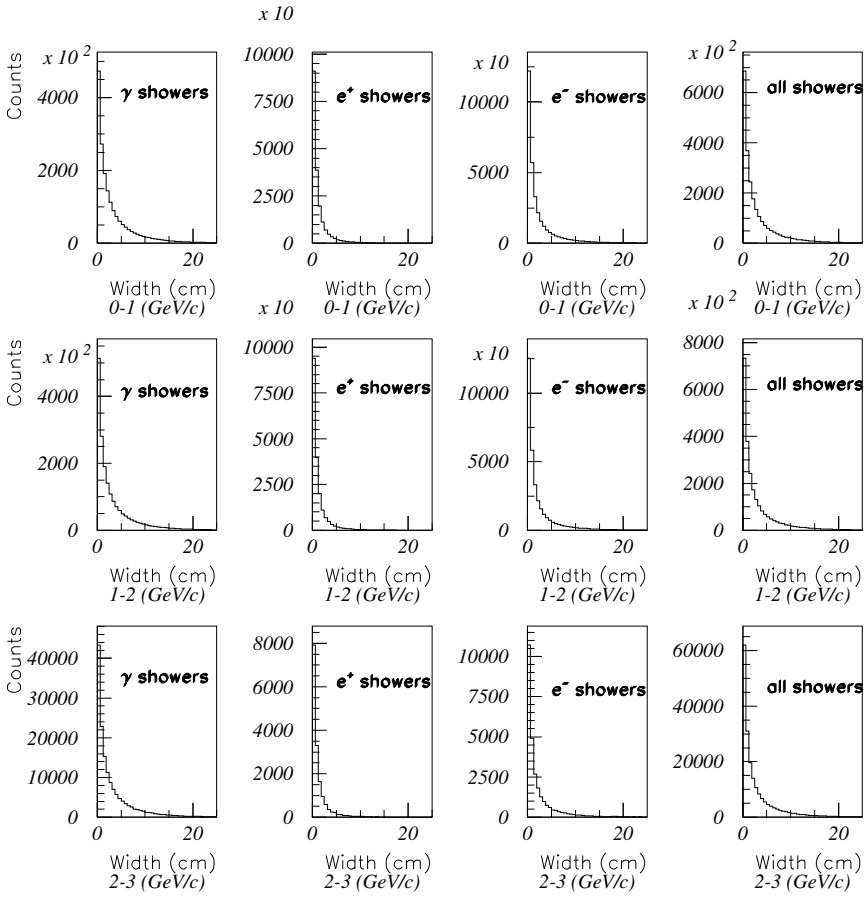

Figure 14: The following plots depict the width of specific shower particles and all shower particles combined in the ECs for specific momentum ranges (GeV/c). These showers were initiated by gammas.

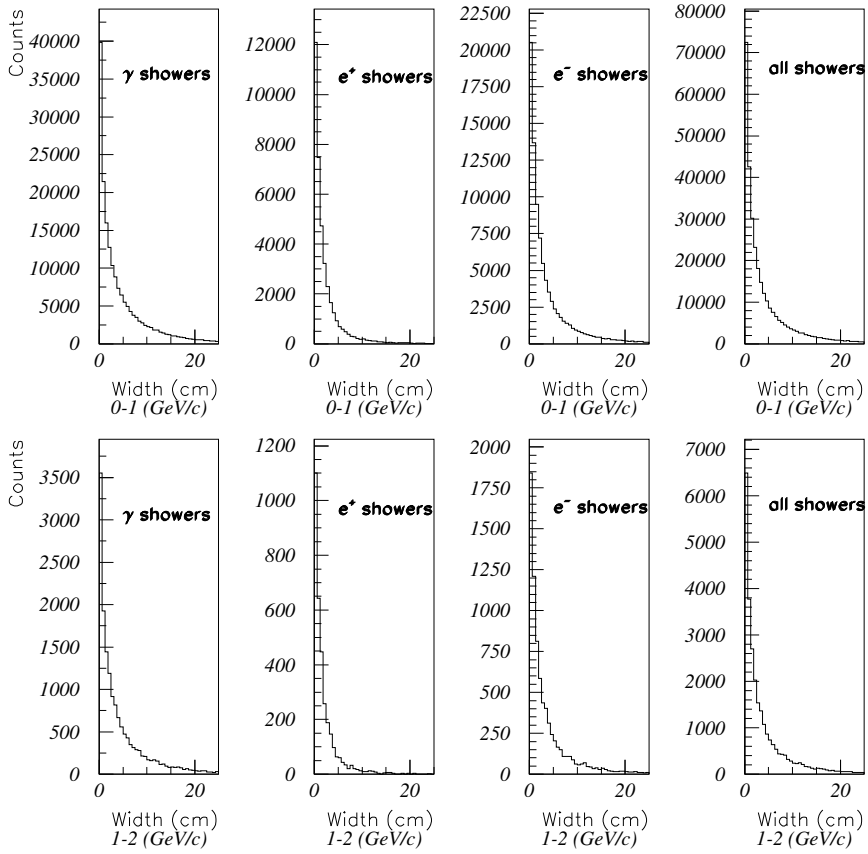

Figure 15: The following plots depict the width of specific shower particles and all shower particles combined in the LACs for specific momentum ranges (GeV/c). These showers were initiated by gammas.

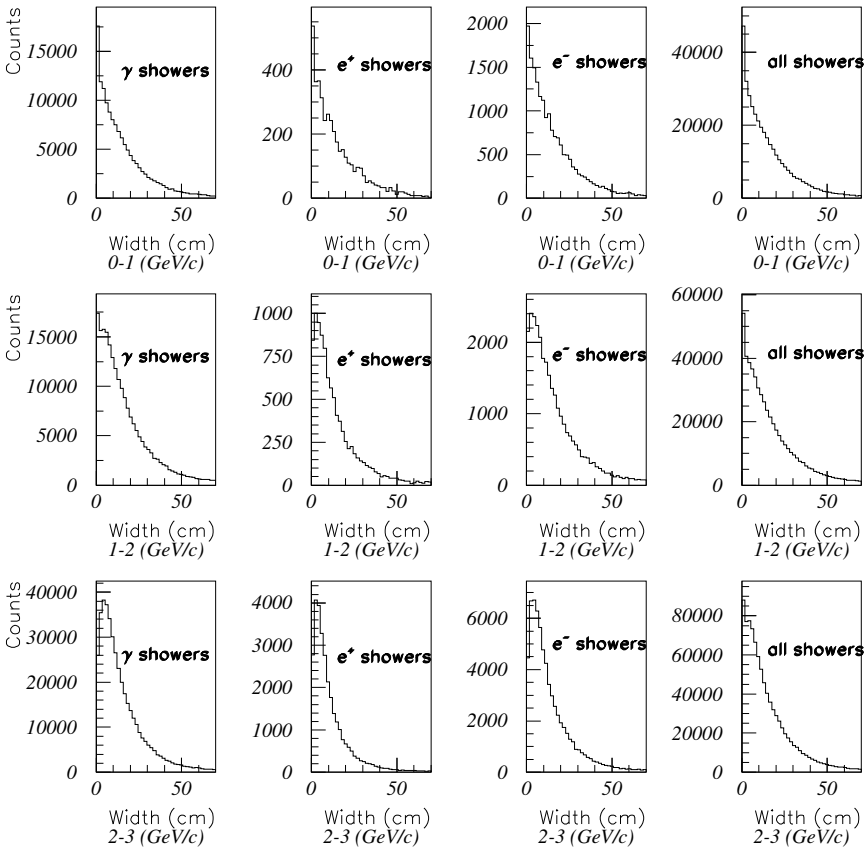

Figure 16: The following plots depict the width of specific shower particles and all shower particles combined in the ECs for specific momentum ranges (GeV/c). These showers were initiated by neutrons.

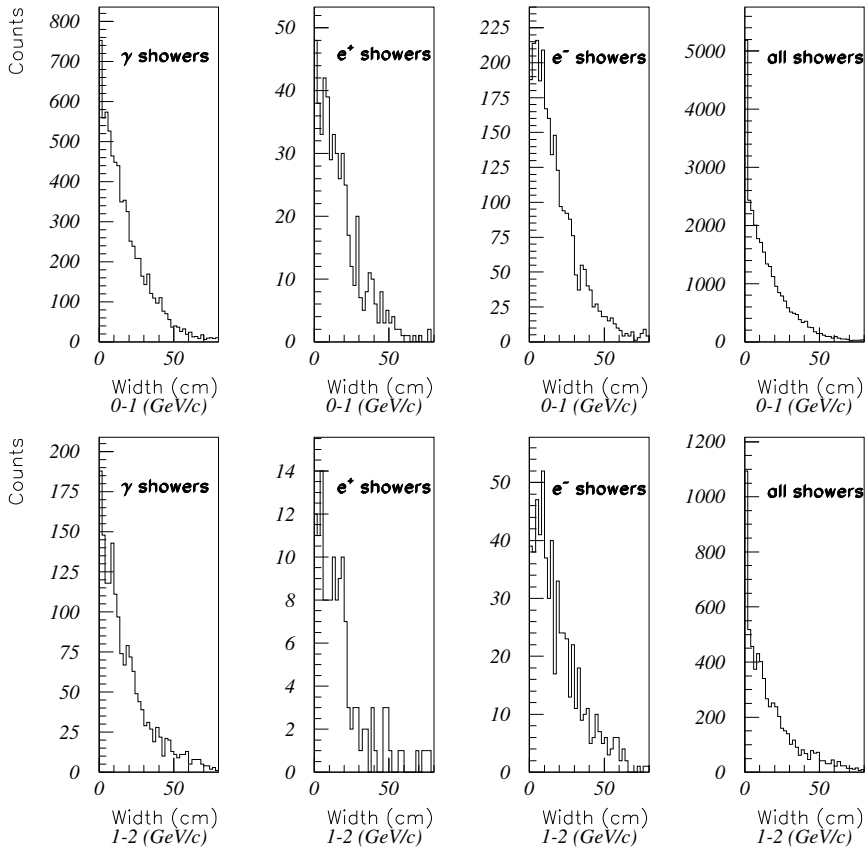

Figure 17: The following plots depict the width of specific shower particles and all shower particles combined in the LACs for specific momentum ranges (GeV/c). These showers were initiated by neutrons

From the projections Fig. 14 - 17 and the tables (1) and (2) a definite difference between showers initiated by γ-rays and neutrons becomes evident for both the ECs and LACs. Showers caused by γ-rays on average have much smaller shower widths in comparison to neutrons. This holds true for both the individual components in the showers such as photons, e^+, and e^- and the entire composition of the shower. For instance, notice between 2-3 GeV/c the showers initiated on by γ-rays in the ECs had an average entire shower width of 6.1 cm. While a neutron initiating a shower in the ECs for the exact same absolute momentum range would have an average shower width of 21.0 cm.

Although interesting, experimentally it is impossible to distinguish between individual shower particles as in Tables (1) and (2). Instead it is more appropriate to analyze the average width of an entire shower caused by a particular shower initiating particle as in Table (3). The average widths and RMS values in Table (3) were determined by the projections from Fig. 18, 19, and 20 for showers in the ECs, while the statistics for the LACs were determined by the average distributions in Fig. 21 and 22. For comparison, other charged hadrons and mesons that initiate showers from reactions (2) - (4) are also included.

			Width (cm)				
			ECs			**LACs**	
Reaction	Particle	Statistic	**Low**	**Med**	**High**	**Low**	**Med**
2	γ	AVG	6.1	6.0	4.3	5.3	5.1
		RMS	5.1	4.8	6.3	3.9	6.9
2	p	AVG	21.1	21.7	19.0	17.9	18.5
		RMS	37.5	35.0	29.1	28.9	24.2
3	n	AVG	21.4	22.6	20.1	17.7	20.0
		RMS	37.8	35.0	33.0	24.1	29.1
3	π^+	AVG	20.6	18.5	17.3	18.5	18.0
		RMS	33.9	29.1	24.5	24.7	21.4
4	p	AVG	19.9	22.1	18.8	17.9	17.2
		RMS	38.4	35.8	27.9	29.4	25.7
4	π^+	AVG	18.3	18.1	19.8	16.5	17.8
		RMS	33.4	28.2	24.6	21.1	26.2
4	π^-	AVG	17.9	20.6	23.6	17.4	22.9
		RMS	29.4	35.8	36.6	28.2	40.7

Table 3: The average width of showers (cm) in the ECs and LACs caused by all shower initiating particles from reactions (2), (3), and (4).

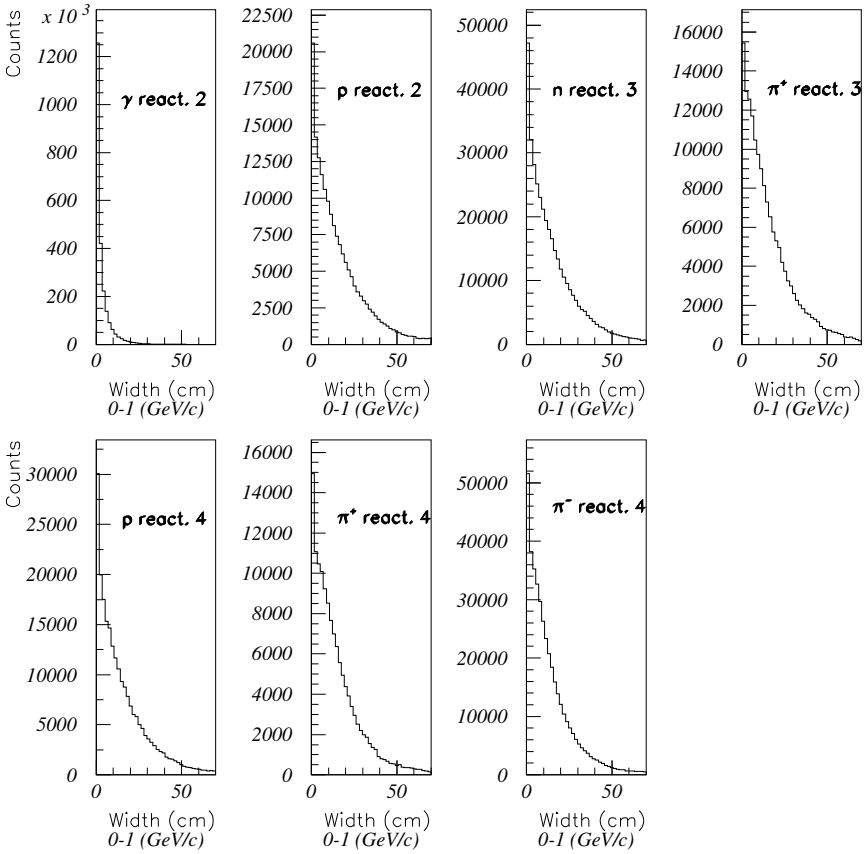

Figure 18: The following plots depict the width of all shower particles combined in the ECs for the momentum range of 0-1 (GeV/c). These showers were initiated by the particles specified in the plot.

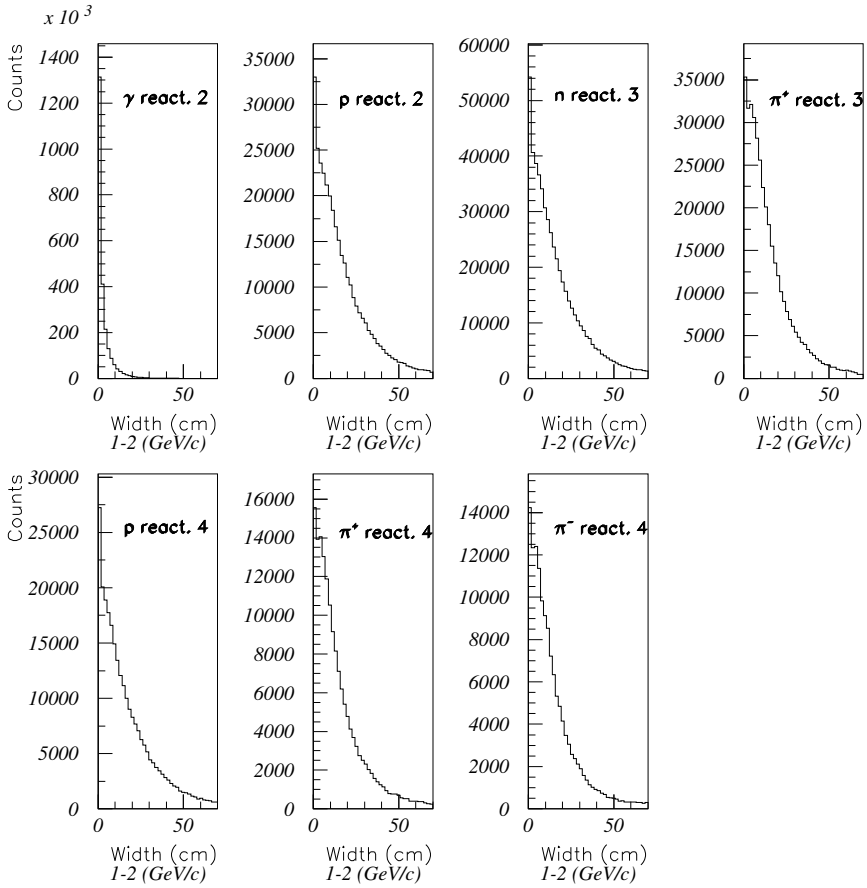

Figure 19: The following plots depict the width of all shower particles combined in the ECs for the momentum range of 1-2 (GeV/c). These showers were initiated by the particles specified in the plot.

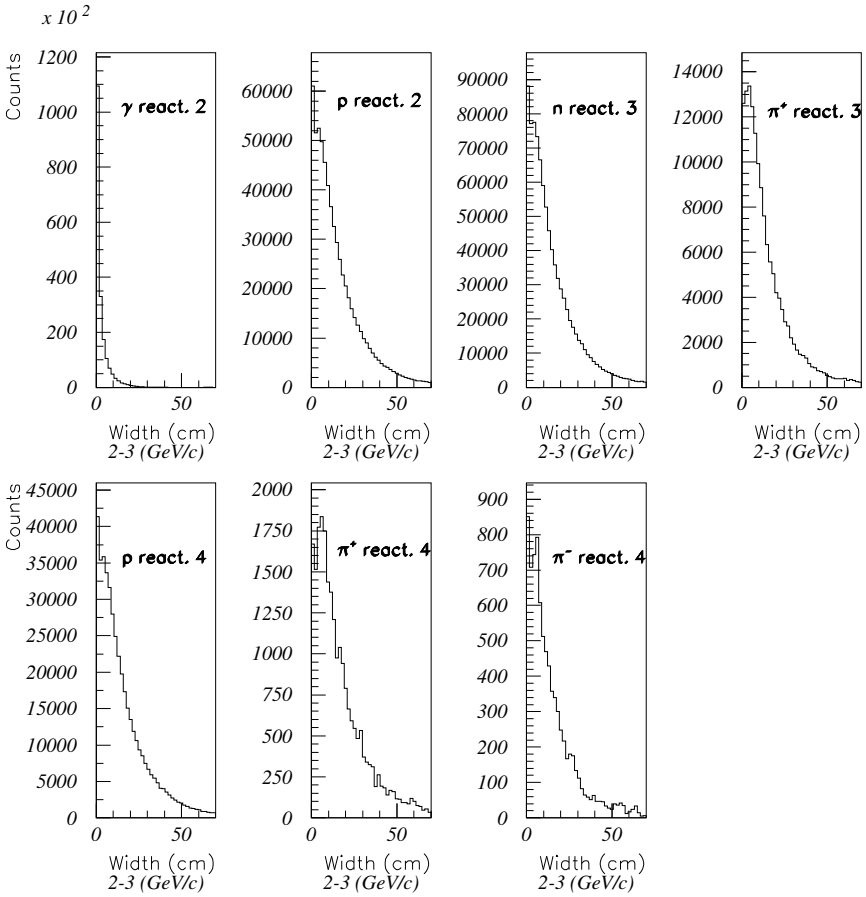

Figure 20: The following plots depict the width of all shower particles combined in the ECs for the momentum range of 2-3 (GeV/c). These showers were initiated by the particles specified in the plot.

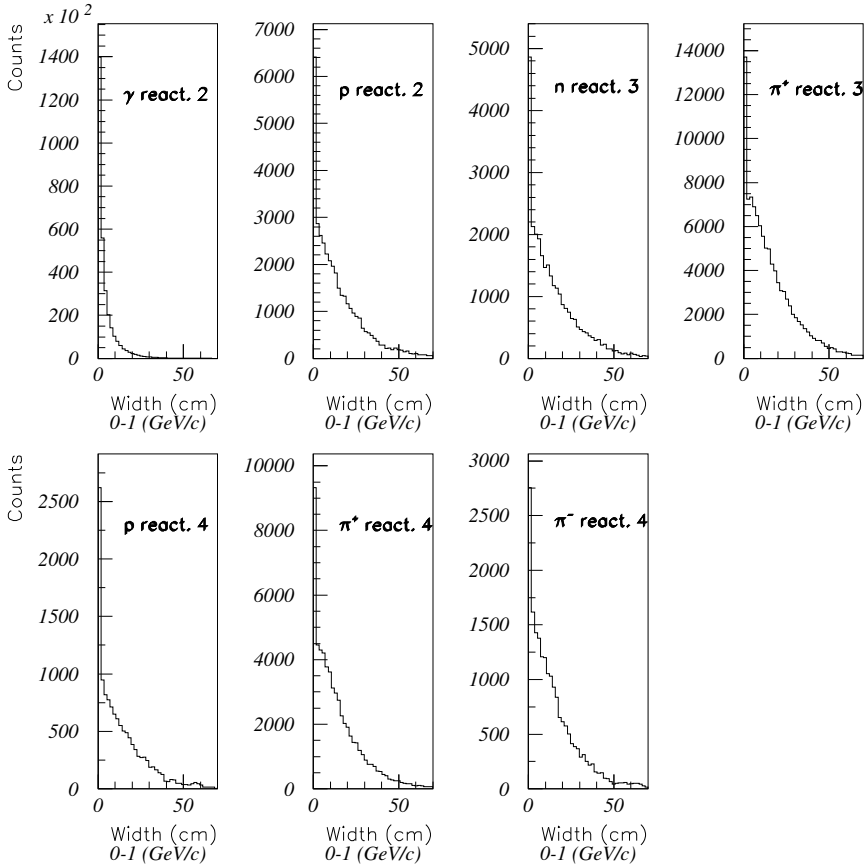

Figure 21: The following plots depict the width of all shower particles combined in the LACs for the momentum range of 0-1 (GeV/c). These showers were initiated by the particles specified in the plot.

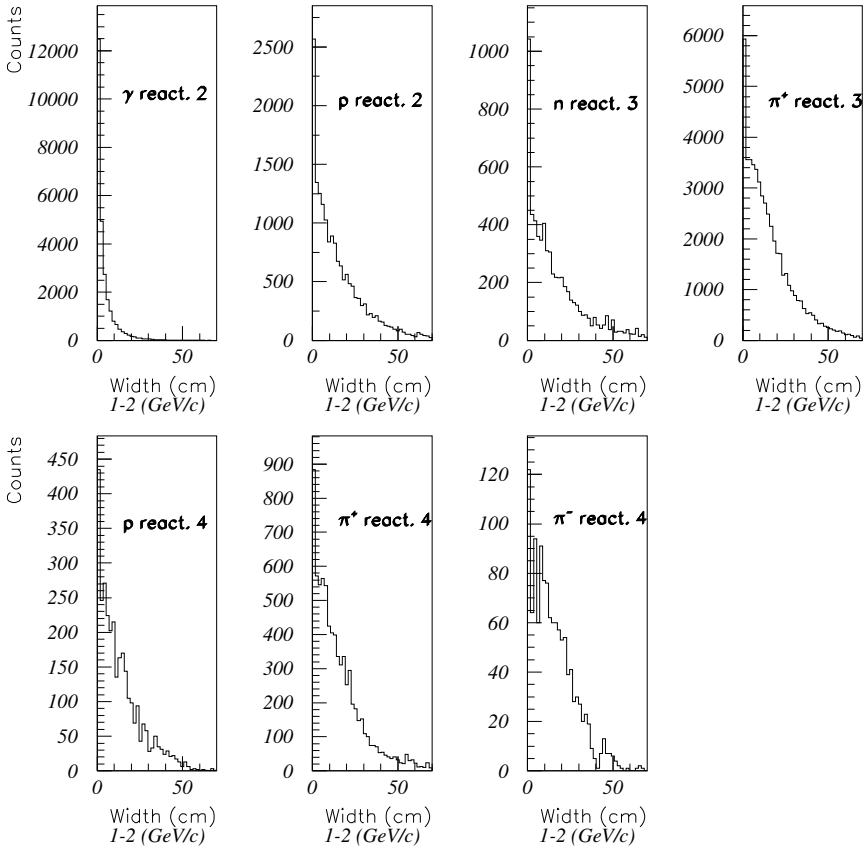

Figure 22: The following plots depict the width of all shower particles combined in the LACs for the momentum range of 1-2 (GeV/c). These showers were initiated by the particles specified in the plot.

It is evident that γ-rays produced showers with much smaller FWHM average shower widths in comparison to neutrons, protons, and pions. This result is important because it means that the shower particle width is an effective means to distinguish between γ initiated showers in comparison to neutron showers in the ECs and LACs. The ECs are composed of 1 cm thick BC412 scintillators that have a projective width of 10 cm [AMAR01]. While the LACs consist of 1.5 cm thick NE100A plastic scintillators with a projective width of 10 cm [MECK03]. From Table (3) it is evident that an average γ-ray shower would fit on one scintillator paddle, although the same γ-ray shower could be spread between two scintillator paddles in smaller proportions if the shower occurred near the edge of the paddle. This finding applies to γ-ray showers in both the ECs and LACs. It represents a promising result for n-γ discrimination since the average neutron shower must occur on at least two if not three scintillator paddles for both the ECs and LACs according to the results of Table (3). The same result for neutrons also holds true for pions and protons. Therefore, shower width provides an effective means to discriminate between hadronic and EM showers in both the ECs and LACs of CLAS.

9 Analysis of shower particle scatter angle

A shower scattering angle was defined as the angle between the initial shower particle momentum at the end of its track and the momenta of all shower particles. An example of this angle is shown in the flow diagram of Fig. 23.

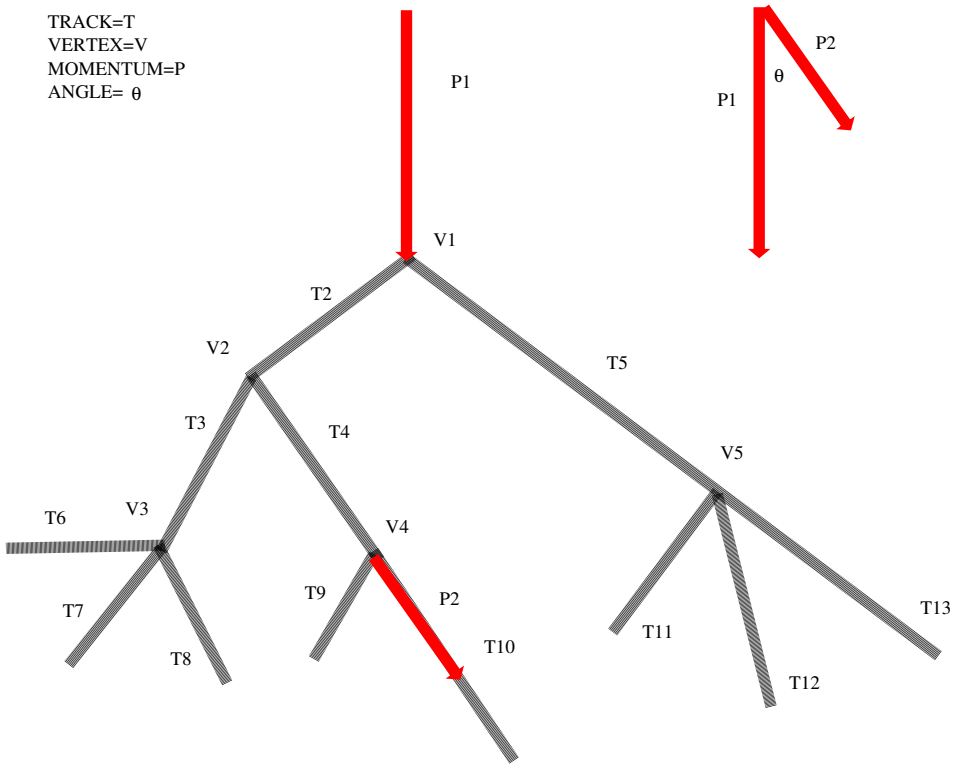

Figure 23: This diagram shows the scattering angle of a shower particle. This quantity is defined as the angle between the 3-momentum of the initial particle causing an interaction vertex at the end of a track and the 3-momentum of the shower particle when it is detected as a hit. This allows the examination of the angular range of a shower that is independent of the width of the shower but dependent on momentum of the shower.

This shower particle scattering angle constitutes another excellent variable for discriminating between γ-ray and neutron initiated showers. The momentum of the shower initiating particle can be plotted against the shower scattering angle of the cascading particles as in Fig. 24 and 25 for the EC and LAC respectively. Then one can make shower angle projections for "low" (0-1 GeV/c), "medium" (1-2 GeV/c), and "high" (2-3 GeV/c) momentum bins as seen in Fig. 26 - 28 for the ECs and Fig. 29 - 30 for the LACs. The averages and RMS values of these projections are displayed in Table (4).

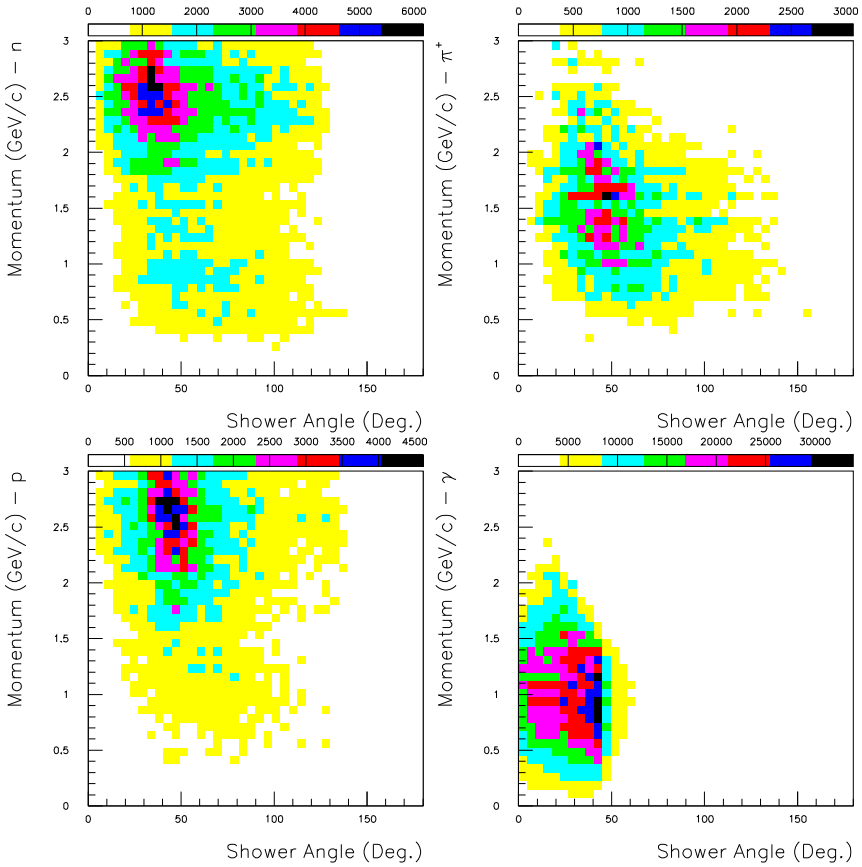

Figure 24: The showers in this diagram are initiated by the products of reaction (2) and (3) in the EC. A range of shower scattering angles are plotted against a reaction product particle momentum range of (0-3) GeV/c. The reaction product particles causing the showers are n, π^+, p, and γ particles in the top left, top right, bottom left, and bottom right respectively.

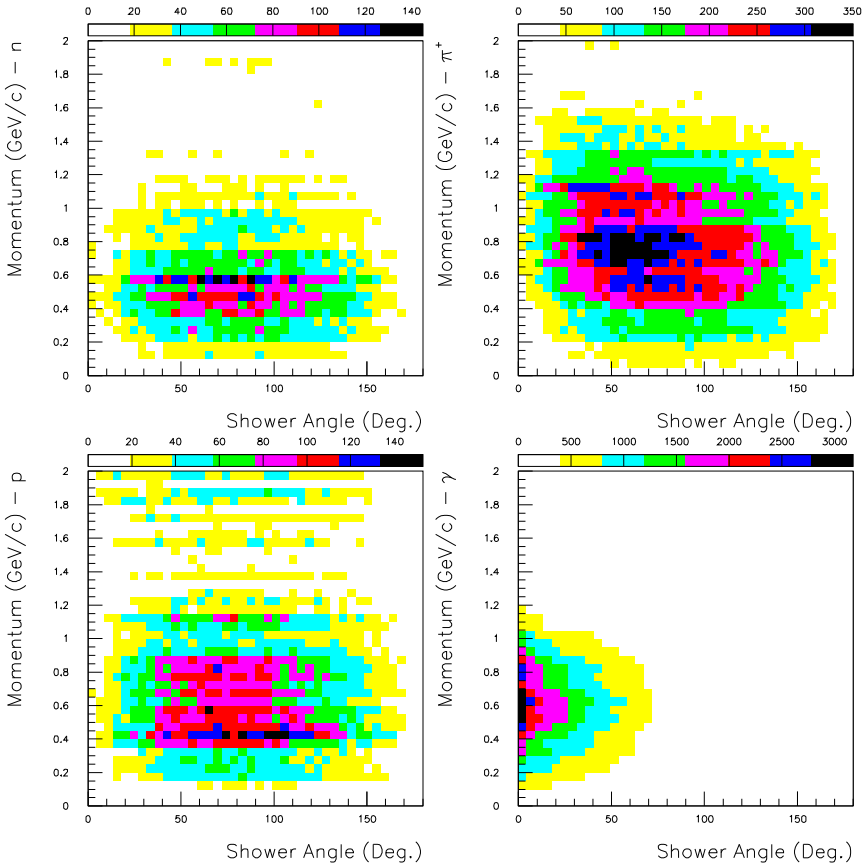

Figure 25: The showers in this diagram are initiated by the products of reaction (2) and (3) in the LAC. A range of shower scattering angles are plotted against a reaction product particle momentum range of (0-2) GeV/c. The reaction product particles causing the showers are n, π^+, p, and γ particles in the top left, top right, bottom left, and bottom right respectively.

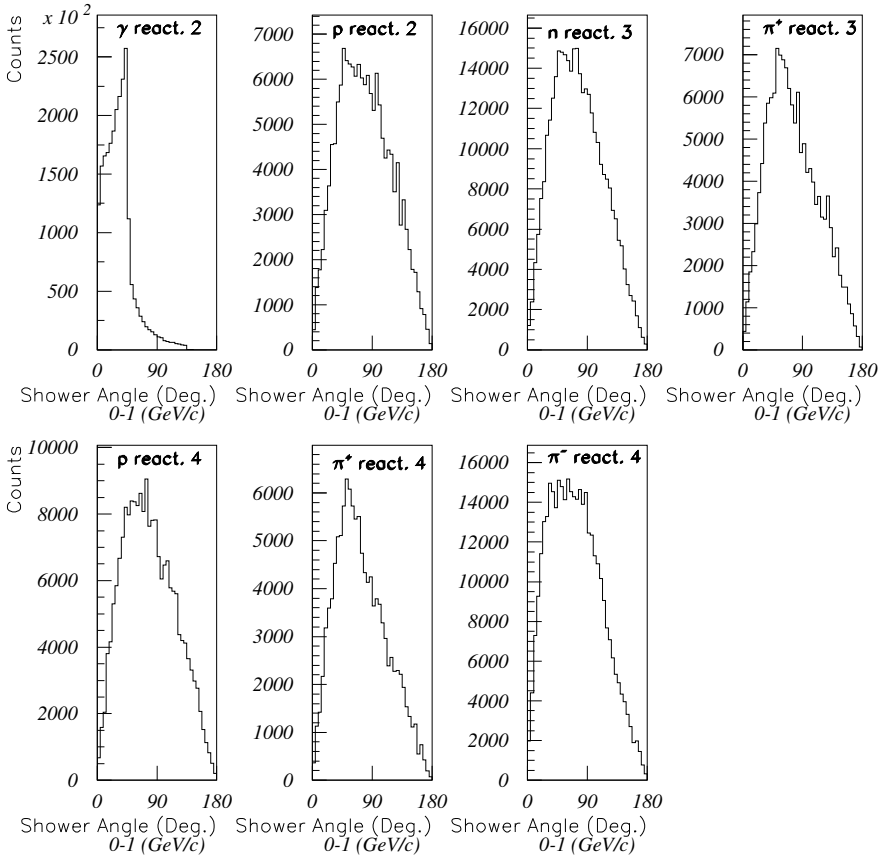

Figure 26: The following plots depict the shower angle of all shower particles combined in the ECs from 0-1 (GeV/c). These showers were initiated by the products from reactions (2) - (4).

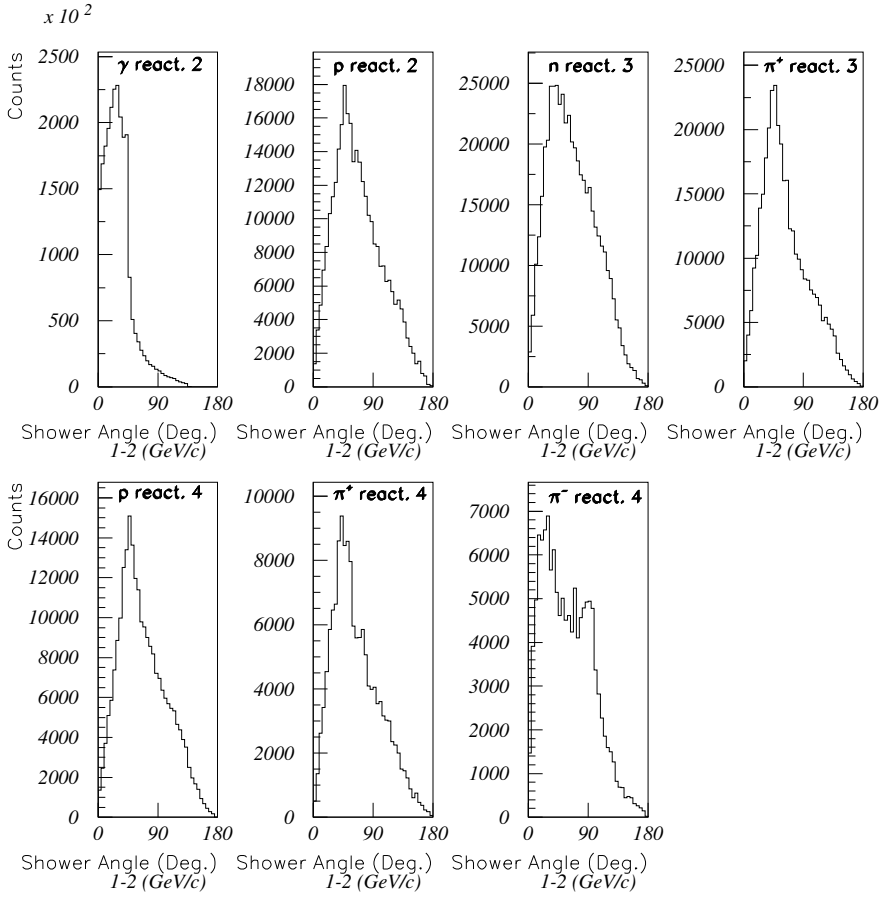

Figure 27: The following plots depict the shower angle of all shower particles combined in the ECs from 1-2 (GeV/c). These showers were initiated by the products from reactions (2) - (4).

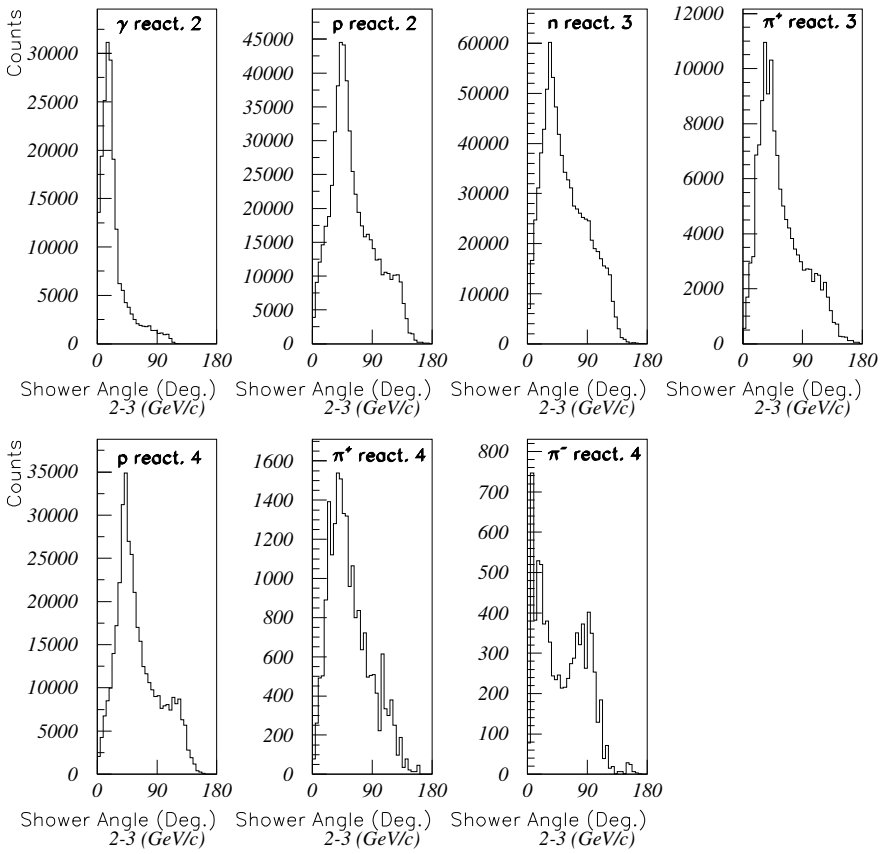

Figure 28: The following plots depict the shower angle of all shower particles combined in the ECs from 2-3 (GeV/c). These showers were initiated by the products from reactions (2) - (4).

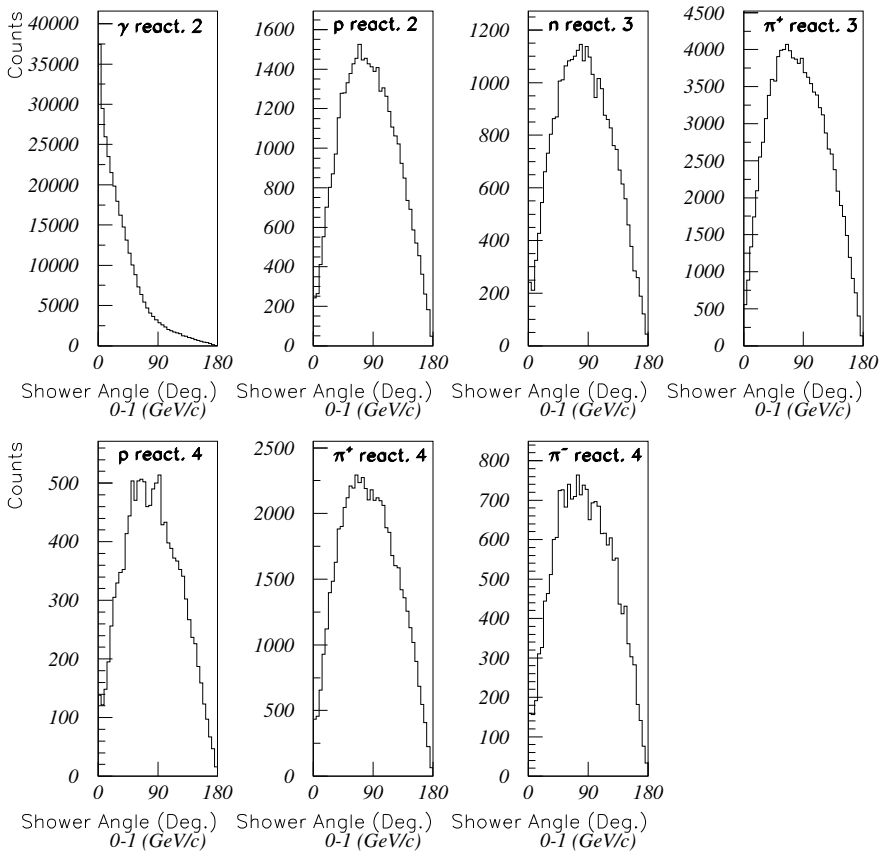

Figure 29: The following plots depict the shower angle of all shower particles combined in the LACs from 0-1 (GeV/c). These showers were initiated by the products from reactions (2) - (4).

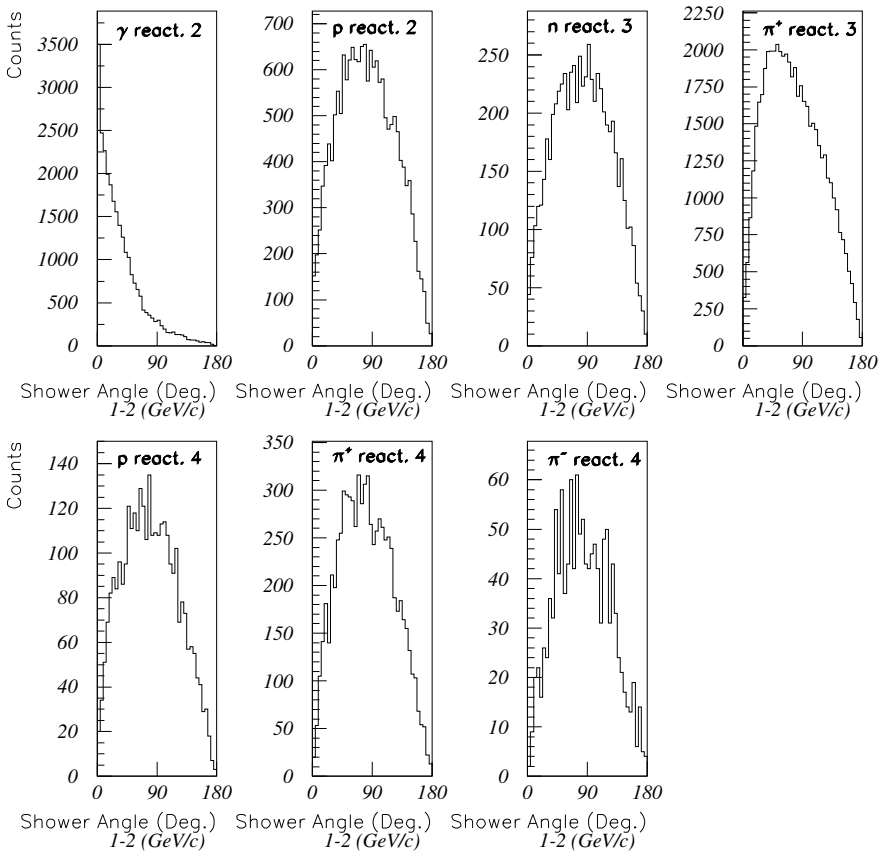

Figure 30: The following plots depict the shower angle of all shower particles combined in the LACs from 1-2 (GeV/c). These showers were initiated by the products from reactions (2) - (4).

			Shower Angle (Deg.)				
			ECs			**LACs**	
Reaction	Particle	Statistic	**Low**	**Med**	**High**	**Low**	**Med**
2	γ	AVG	32.8	30.8	25.1	35.5	35.3
		RMS	22.0	21.9	21.5	32.7	32.9
2	p	AVG	79.6	68.4	61.6	82.1	81.8
		RMS	38.8	36.1	33.7	40.2	41.3
3	n	AVG	76.6	66.1	57.3	83.7	83.9
		RMS	37.7	35.4	33.0	40.3	41.4
3	π^+	AVG	76.1	63.7	57.4	82.7	77.2
		RMS	38.2	34.9	33.4	40.6	41.2
4	p	AVG	78.3	67.7	61.7	81.7	80.3
		RMS	38.7	35.3	33.0	40.2	40.7
4	π^+	AVG	73.5	65.0	56.8	83.6	82.1
		RMS	37.6	35.2	31.1	40.6	39.9
4	π^-	AVG	72.3	59.6	53.0	84.9	83.8
		RMS	38.6	36.4	34.9	40.9	39.6

Table 4: The shower angle (Deg.) of particles in the ECs and LACs caused by the products of reactions (2), (3), and (4) respectively.

From the projections in Fig. 26 - 30 and the statistics in table (4), it is evident that the scattering angle of the showering particles is a good characteristic for distinguishing between an EM and a hadronic shower in the ECs and LACs. The γ-rays were shown to produce showers with average scattering angles roughly two times less than neutrons in the ECs and LACs. This provides another variable to distinguish between γ-ray and neutron initiated showers in CLAS. This result also agrees with the fact that γ-ray initiated shower particles were shown to have significantly smaller shower widths than neutrons, protons, and pions.

10 Summary and outlook

The shower topology appears to be a worthy choice for studying the EC and LAC detectors. It presents a promising method for distinguishing between a hadronic shower and an EM shower and could be complementary

when combined with time-of-flight data. The absence of hadrons in EM γ-ray initiated showers is likely the primary cause of this unique topology. With further improvements to the analysis program, energy loss statistics could also be an area of future investigation. This topology analysis which focuses on shower width and scattering angle is particularly successful in distinguishing between neutrons and gamma rays. The average γ-ray initiated shower was shown to fit on one to two paddles and the average neutron initiated shower was shown to fit on two to three paddles in the ECs and LACs. As well, a γ-ray initiated shower is shown to produce a shower with scattering angles that are roughly half that of a neutron shower. From the analysis, it is evident that EM showers have much smaller average shower widths in comparison to hadronic showers. Thus, the preceding method could also be used to support e^- and pion separation. This extension would be comprehensive in addition to identification by the Čerenkov Counters. The main structure of the program has been created, which makes future developments relatively straightforward and will be included in the upcoming single pion analysis [JUEN03].

11 Acknowledgments

Foremost, I would like to thank my summer research supervisor at the Jefferson Laboratory, Dr. Henry G. Juengst, for his time and tireless efforts in educating me throughout the summer. His assistance and guidance was greatly appreciated. I would also like to thank Dr. James W. Jury for giving me the opportunity to be a part of his Trent University research group over the past year. Through his generosity I was given an undergraduate research position at one of the leading nuclear facilities in the United States. Finally, I would like to thank Dr. Barry L. Berman and Dr. William J. Briscoe from the George Washington University for their support and allowing me the privilege to work with their group over the summer at the Jefferson Laboratory. My summer work was kindly assisted by an Undergraduate Summer Research Assistantship (URSA) award granted by the Natural Sciences and Engineering Council of Canada (NSERC).

References

[FABJ03] C.W. Fabjan, F. Gianotti
Calorimetry for Particle Physics, Reviews of Modern Physics, 75, 1243-1284 (2003)

[ANZI93] G. Anzivino et al.
Electron-Pion Discrimination With Projective Lead/Scintillating Fibers Calorimeters, Proceedings of the Fourth International Conference on Calorimetry in High Energy Physics, World Scientific, 226-229 (1994)

[JUEN03] H.G. Juengst
Private Communication. July/August 2003

[BRUY86] F. Bruyant
GEANT3 User's Guide, CERN, HITS 001, 1-3, (1986)

[GROO00] D.E. Groom et al.
Particle Physics Booklet, The European Physical Journal C, 1, 15 (2000)

[AMAR01] M. Amarian et al.
The CLAS Forward Electromagnetic Calorimeter, Nuclear Instruments and Methods in Physics Research A, 460, 239-265 (2001)

[MECK03] B. Mecking et al.
The CEBAF large acceptance spectrometer (CLAS), Nuclear Instruments and Methods in Physics Research A, 503, 513-553 (2003)

[HAGI02] B. K. Hagiwara et al.
The Review of Particle Physics, Physical Review. D, 66, 010001 (2002)